A Model for Effector Activity in a Highly Specific Biological Electron Transfer Complex: The Cytochrome $P450_{cam}$−Putidaredoxin Couple[†,‡]

Susan Sondej Pochapsky,[§] Thomas C. Pochapsky,* and Julie W. Wei[§]

Department of Chemistry, Brandeis University, 415 South Street, MS 015, Waltham, Massachusetts 02454-9110

Received February 18, 2003; Revised Manuscript Received March 31, 2003

ABSTRACT: The camphor hydroxylase cytochrome $P450_{cam}$ (CYP101) catalyzes the 5-exo hydroxylation of camphor in the first step of camphor catabolism by *Pseudomonas putida*. CYP101 forms a specific electron transfer complex with its physiological reductant, the $Cys_4Fe_2S_2$ ferredoxin putidaredoxin (Pdx). Pdx, along with other proteins and small molecules, has also been shown to be an effector for turnover by CYP101. Multidimensional nuclear magnetic resonance (NMR) techniques have been used to make extensive sequential ^1H, ^{15}N, and ^{13}C resonance assignments in CYP101 that permit a more complete characterization of the complex formed by CYP101 and Pdx. NMR-detected perturbations in CYP101 upon Pdx binding encompass regions of the CYP101 remote from the putative Pdx binding site, including in particular a region of the CYP101 molecule that has been implicated in substrate access to the active site via dynamical processes. A model for effector activity is proposed in which the primary role of the effector is to prevent uncoupling (formation of reduced oxo species without formation of hydroxycamphor) by enforcing conformations of CYP101 that prevent loss of substrate and/or intermediates prior to turnover. A secondary role could also be to enforce conformations that permit efficient proton transfer into the active site for coupled proton/electron transfer.

Cytochrome P450s are heme-containing enzymes that catalyze the insertion of one oxygen atom from O_2 into unactivated C−H bonds with concomitant two-electron reduction of the other oxygen atom to water (Figure 1). Cytochrome $P450_{cam}$ (CYP101)[1] catalyzes the 5-exo hydroxylation of camphor, the first step of camphor catabolism by the soil bacterium *Pseudomonas putida* (*1*). The two electrons required for camphor hydroxylation by CYP101 come from the oxidation of NADH, which is catalyzed by putidaredoxin reductase (PdR). These electrons are shuttled from PdR to CYP101 by a $Cys_4Fe_2S_2$ ferredoxin, putidaredoxin (Pdx), in two distinct electron transfer events. While the first reduction of CYP101 [from Fe(III)S to Fe(II)S, Figure 1] can be accomplished by any reducing agent with a suitable reduction potential, the second reduction requires the presence of an effector in order to result in the formation of a hydroxycamphor product (*2*). It has been demonstrated kinetically that a complex between O_2−Fe(II)S and an effector (Ef) is the catalytically competent species (*2*). In the absence of such a complex, the O_2−Fe(II)S complex autoxidizes ($k = 0.015$ s^{-1} at 295 K) to yield ferric CYP101 [Fe(III)S] and superoxide ($O_2^{-\bullet}$) (*3*). Although a number of small molecules and negatively charged proteins are effectors

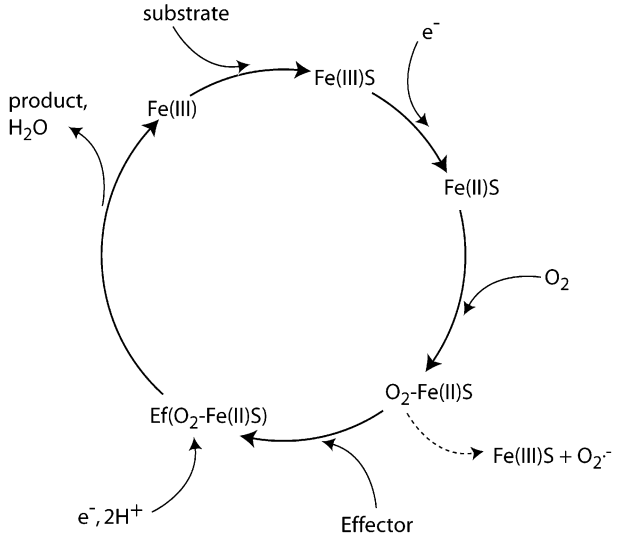

FIGURE 1: Catalytic cycle of CYP101, showing the abbreviations for various forms of CYP101 used in the text. The abbreviations are as follows: Fe(III), resting state Fe^{3+} CYP101; Fe(III)S, substrate-bound Fe^{3+} CYP101; Fe(II)S, substrate-bound Fe^{2+} CYP101; O_2−Fe(II)S, dioxygen- and substrate-bound Fe^{2+} CYP101; Ef[O_2−Fe(II)S], effector complex with O_2−Fe(II)S.

[†] This work was supported by a grant from the National Institutes of Health, R01-GM44191 (to T.C.P.).

[‡] Resonance assignments for CYP101 have been deposited with the BMRB database (www.bmrb.wisc.edu), accession number 5759.

* Address correspondence to this author. E-mail: pochapsk@brandeis.edu. Website: http://www.chem.brandeis.edu/pochapsky. Phone: 781-736-2559. Fax: 781-736-2516.

[§] Both of these authors contributed equally to the work.

[1] Abbreviations: Adx, adrenodoxin; CO−Fe(II)S, carbon monoxide and camphor-bound oxidized cytochrome $P450_{cam}$; CYP101, cytochrome $P450_{cam}$; DTT, dithiothreitol; Ef, effector; Fe(III)S, camphor-bound oxidized cytochrome $P450_{cam}$; IPTG, isopropyl β-D-thiogalactoside; LB, Luria−Bertani media; NMR, nuclear magnetic resonance; NOE, nuclear Overhauser effect; NOESY, NOE spectroscopy; HSQC, heteronuclear single-quantum correlation; M9, minimal growth medium; MALDI-TOF, matrix-assisted laser desorption ionization−time of flight mass spectrometry; O_2−Fe(II)S, carbon monoxide and camphor-bound oxidized cytochrome $P450_{cam}$; PdR, putidaredoxin reductase; Pdx^o, oxidized putidaredoxin; Pdx^r, reduced putidaredoxin; rms, root mean square; Tdx, terpredoxin; TPPI, time-proportional phase incrementation; TROSY, transverse relaxation optimized spectroscopy; WT, wild type; 2D, two dimensional; 3D, three dimensional.

10.1021/bi034263s CCC: $25.00
Published on Web 04/25/2003

for CYP101, the physiological reductant Pdx is the in vivo effector (*2*).

The interactions between Pdx and CYP101 are quite specific. Homologous ferredoxins adrenodoxin (Adx) and terpredoxin (Tdx) do not support turnover in the CYP101 system (*2*, *4*). Modeling and experiment have provided insight into the nature of the specific interactions between Pdx and CYP101 (*5*−*8*). The binding of Pdx to CYP101 results in spectral perturbations to heme-linked transitions in CYP101 (*9*−*11*). Resonance Raman spectra show that the binding of reduced Pdx (Pdx^r) to reduced CO- and NO-bound Fe(II)S results in changes in the electronic and/or structural environment of the proximal cysteine ligand and the porphyrin ring (*12*). It has been suggested that these perturbations are related to the effector activity of Pdx and may alter the electron-donating nature of the axial thiolate ligand (*12*, *13*). Still, a number of observations argue against a heme-localized model of effector activity or one that directly affects electron transfer rates. Cytochrome b_5, which is an effector for CYP101 turnover, does not cause the same types of spectral changes in CYP101 that are associated with Pdx binding (*12*). This suggests that the localized changes in the heme environment observed upon binding of Pdx are not critical for effector activity. Also, the effectors identified for CYP101 turnover besides Pdx are by and large not capable of donating electrons to that enzyme; either their redox potentials are not appropriate or they contain no redox center (*14*). As such, effector activity must be separate from electron transfer, and perturbations in the active site associated with Pdx binding, while perhaps advantageous for rapid electron transfer, seem unlikely to be the primary cause of effector activity. Taken together, these observations suggest that the origins of effector activity are as yet unknown.

To obtain a more detailed picture of the interactions between Pdx and CYP101, we have applied multidimensional nuclear magnetic resonance (NMR) methods to the characterization of the CYP101/Pdx complex. NMR methods have been previously used to investigate this complex from the point of view of Pdx (*6*, *15*), but CYP101 is a bigger challenge for the spectroscopist (*16*−*18*). Until the advent of TROSY-based NMR methods designed for use with large proteins (*19*) it would have been difficult to imagine tackling the problem of sequence-specific assignments in the monomeric 414-residue CYP101. However, using a series of perdeuterated uniformly and selectively ^{13}C- and ^{15}N-labeled samples of CYP101, we have now made extensive sequential ^1H, ^{15}N, and ^{13}C resonance assignments in CYP101. Using these assignments, we have monitored perturbations in the CYP101 structure upon addition of Pdx, and we propose a model for the effector activity of Pdx consistent with our own and other published experimental observations on the CYP101/Pdx couple.

MATERIALS AND METHODS

Protein Expression and Purification. Perdeuterated [U-^{13}C,^{15}N]CYP101 was expressed in *Escherichia coli* strain NCM533 transformed with a plasmid construct encoding the C334A mutant of CYP101 under the control of the *lac* promotor. The C334A mutant has been shown to be spectroscopically and enzymatically identical to wild-type enzyme but does not form dimers in solution (*20*). The inoculant was grown in M9 medium supplemented with trace metals (M9+) to an OD_{600} of 1.0. The cells were then transferred into 100% D_2O M9+ media prepared using uniformly ^{13}C-labeled glycerol and $^{15}NH_4Cl$. Protein expression was induced with 1 mM IPTG when the OD_{600} reached 1.0 and harvested after 24 h.

Purification of CYP101 followed published procedures, with the inclusion of a protamine sulfate−nucleic acid precipitation and the exclusion of the ammonium sulfate precipitation. Typically, 1 L of growth medium produces 11 mg of CYP101. Pdx was expressed and purified as described previously (*21*). Bovine Adx was expressed and purified according to published methods (*22*). The bacterially expressed soluble fragment of rat cytochrome b_5 was obtained in purified form from Prof. J. T. J. LeComte (Pennsylvania State University). The purities of CYP101, Pdx, and Adx were determined by measuring absorption ratios at A_{390}/A_{275}, A_{325}/A_{280}, and A_{414}/A_{276}, respectively, on a Hitachi U-2000 UV−visible spectrometer. CYP101 (0.5 mM) of 1.4 absorption ratio, Pdx (3.5 mM) of 0.55 absorption ratio, and Adx (1.8 mM) of 0.6 absorption ratio were used for NMR experiments. The level of deuteration of CYP101 was ca. 85% as measured by mass spectrometry. NMR samples were prepared by concentrating samples using Amicon (Millipore) centrifugal concentrators and then passing samples through buffer exchange resins preequilibrated with NMR buffer.

Reduction of CYP101, Pdx, Adx, and Rat Cytochrome b_5. Samples of reduced CO-bound CYP101 [CO−Fe(II)S] were prepared as follows. Two hundred microliters of 0.5 mM [U-^{15}N]CYP101 was placed in a CO atmosphere for 15 min and then reduced with 8 μL of 0.25 M $Na_2S_2O_4$ prepared in degassed 1 M Tris-HCl (pH 8.0). The reduced sample remained under CO for an additional 2 min before anaerobic transfer to an NMR sample tube (Shigemi). Reduced samples of Pdx were prepared as follows. Two hundred fifty microliters of Pdx was concentrated to 3.95 mM in an anaerobic chamber and then reduced with 10 μL of 1 M $Na_2S_2O_4$ prepared as described above. Bovine Adx and soluble rat cytochrome b_5 samples were concentrated and reduced in a similar fashion, using 20 and 10 μL of reducing agent, respectively.

NMR Spectroscopy. CYP101 samples for all NMR experiments were 0.2−0.65 mM in 90% H_2O/10% D_2O, pH 7.4, 50 mM Tris-*d*-HCl, 150 mM KCl, and 1 mM *d*-camphor. All NMR experiments were performed on a Varian Inova 600 MHz spectrometer, except for the two-dimensional HNCO experiment which was performed on a Varian Inova 500 MHz spectrometer. The Inova 600 operates at 599.702, 150.812, and 60.774 MHz for ^1H, ^{13}C, and ^{15}N, respectively, and is equipped with a dedicated ^2H RF channel (92.06 MHz) for ^2H decoupling, a pulsed field gradient amplifier, and a 5 mm $^1H\{^{13}C,^{15}N\}$ triple resonance PFG probe. The Inova 500 (operating at 499.708, 125.67, and 50.68 MHz) has a similar configuration. All NMR experiments were performed at 35 °C except for the titration with Pdx, which was performed at 17 °C to avoid thermal decomposition of the Pdx.

Oxidized Camphor-Bound CYP101 [Fe(III)S]. A ^{15}N,^{13}C,^2H-labeled Fe(III)S sample was used to acquire 3D TROSY-based HNCO, HN(CO)CA, HNCA, and HNCACB spectra. Experiments were run with 16 scans per t_1 point, 512 (^1H) × 32 (^{13}C) × 32 (^{15}N) complex points, and 1 s recycle delays. Spectral widths were 10000 Hz (^1H) and 2600 Hz (^{15}N). ^{13}C

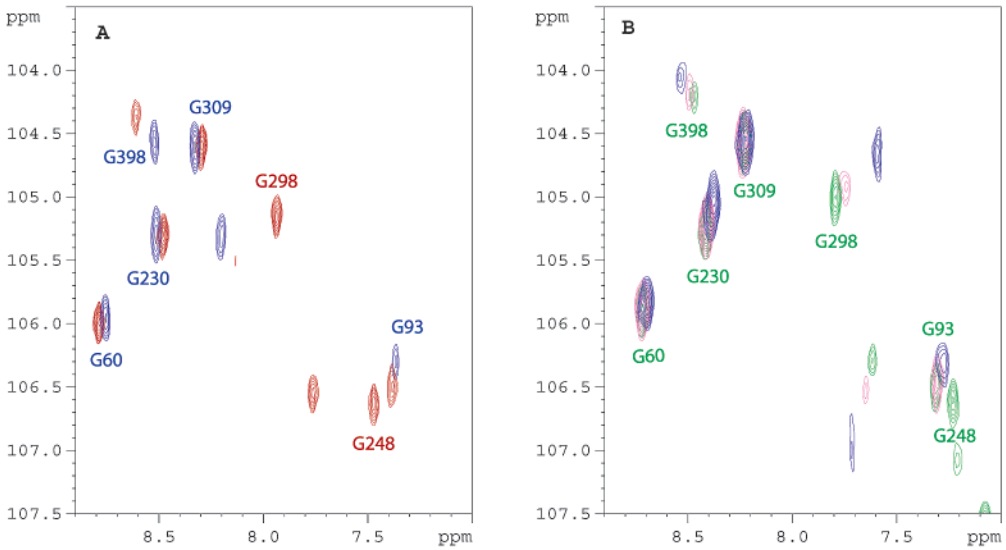

FIGURE 2: (A) Comparison of corresponding regions of ^{15}N, ^{1}H TROSY-HSQC correlation spectra obtained at 600 MHz ^{1}H, 308 K, for oxidized camphor-bound CYP101, Fe(III)S, in blue, and reduced camphor- and CO-bound CYP101, CO−Fe(II)S, in red. Sequential assignments are labeled. Vertical axes are ^{15}N chemical shifts (ppm); horizontal axes are ^{1}H shifts (ppm). Note that some peaks move upon reduction, e.g., Gly 398 (G398), while others, including Gly 248 (G248), are only observed in CO−Fe(II)S. (B) Region of ^{15}N, ^{1}H TROSY-HSQC correlation spectra obtained at 600 MHz ^{1}H, 290 K, showing effects of titration of CO−Fe(II)S with Pdx^{r} upon glycine residues. Peaks are color coded: green corresponds to no Pdx, purple to ~1:5 Pdx:CYP101, and blue to ~2:1 Pdx:CYP101. Resonances corresponding to Gly 60 and Gly 309 are unperturbed by Pdx and Gly 298 and Gly 398 are shifted upon Pdx addition, while Gly 248 is broadened to invisibility after the first addition of Pdx.

spectral widths were 4524 Hz [HNCA and HN(CO)CA], 12064 Hz (HNCACB), and 3000 Hz (HNCO). The implementations of triple resonance experiments used were sensitivity-enhanced gradient coherence selection versions described by Kay et al. (*23*).

A 3D ^{1}H, ^{15}N TROSY-NOESY spectrum and 2D ^{1}H, ^{15}N TROSY-HSQC spectrum were acquired with a ^{2}H,^{15}N-labeled Fe(III)S sample. The HSQC was acquired with spectral widths of 8000 Hz (^{1}H) and 2200 Hz (^{15}N), 640 × 128 complex points, 8 scans per t_1 point, and a 1 s recycle delay. The spectral widths for the 3D NOESY experiment were 10000 Hz (^{1}H), 10000 Hz (^{1}H), and 2000 Hz (^{15}N), with 512 × 128 × 32 complex points, respectively. The mixing time was 150 ms, the recycle delay was 1 s, and 16 scans per t_1 point were acquired.

Reduced Carbon Monoxide- and Camphor-Bound CYP101 [CO−Fe(II)S]. A ^{15}N,^{13}C,^{2}H-labeled CO−Fe(II)S sample was used to acquire 3D TROSY-based HNCA and HNCACB spectra. The same experimental parameters were used as detailed for the Fe(III)S sample, except that the recycle time was 2.1 s. The 2D ^{1}H, ^{15}N TROSY-HSQC and 3D TROSY-NOESY spectra were also acquired using a ^{2}H,^{15}N-labeled CO−Fe(II)S sample. Experimental parameters were the same as for the Fe(III)S sample except the recyle times were 2 s (2D) and 1.3 s (3D).

Selectively Labeled CYP101 Samples. Perdeuterated samples ^{15}N-labeled at one amino acid (leucine, valine, alanine, glycine, threonine, lysine, tyrosine, and glutamate) were used to acquire ^{1}H, ^{15}N TROSY-HSQC spectra of the Fe(III)S and CO−Fe(II)S forms. Scrambling of ^{15}N labels was observed with the [^{15}N]glutamate, [^{15}N]tyrosine, [^{15}N]valine, and [^{15}N]leucine samples. Experiments were run with 512 × 64 complex points, sweep widths of 8000 and 2200 Hz, and 2.7 s recycle times. The number of transients per t_1 point varied between 32 and 256, depending on the concentration of the selectively labeled sample.

A two-dimensional HNCO experiment was performed using a uniformly ^{15}N-labeled and perdeuterated sample of CYP101 in which only the proline carbonyl carbons were labeled with ^{13}C. For this experiment, the ^{1}H and ^{15}N signals evolved in independent time domains, while the carbonyl ^{13}C coherence transfer was used to remove signals of NH groups not bonded to proline carbonyls. The experiment was acquired with 512 × 64 complex points, sweep widths of 8000 and 3000 Hz, and 256 scans per t_1 point.

Titration of CYP101 with Pdx^{r}, Adx^{r}, and Rat Cytochrome b_5. A series of ^{1}H, ^{15}N TROSY-HSQC spectra of a ^{2}H,^{15}N-labeled CO−Fe(II)S sample were acquired at 31, 25, 20, and 17 °C to allow the correlation of our sequential assignments (data acquired at 35 °C) and the titration results (acquired at 17 °C). The titration of CO−Fe(II)S with Pdx^{r} was accomplished by anaerobic addition of aliquots of Pdx^{r} to the CO−Fe(II)S NMR sample. After careful mixing and temperature equilibration at 17 °C in the NMR probe, two ^{15}N, ^{1}H TROSY-HSQC experiments were acquired at each titration point. One was acquired with a standard ^{15}N spectral width (2200 Hz), and the other was acquired with a wider ^{15}N spectral width (4000 Hz) in order to detect the $N_{\epsilon}H$ resonances of arginine residues. All spectra were acquired with 596 (^{1}H) × 128 (^{15}N) complex points, ^{1}H sweep widths of 8000 Hz, 8 scans per t_1 point, and 2.7 s recycle times. Five titration points were used, with final CYP101/Pdx concentrations as follows (in mMs): 0.64/0, 0.618/0.134, 0.588/0.319, 0.544/0.591, and 0.474/1.03. Figure 2 shows comparisons of titration data points in the region of the spectrum showing correlations for glycine residues.

The titration of CO−Fe(II)S with Adx^{r} followed a similar procedure, using an initial Adx concentration of 1.8 mM. The Adx^{r} was added in two aliquots to 160 μL of a 0.2 mM CO−Fe(II)S NMR sample, resulting in ~2:1 and ~5:1 molar ratios of Adx:CYP101. Cytochrome b_5 was added in reduced form to ensure that no unwanted redox processes would take

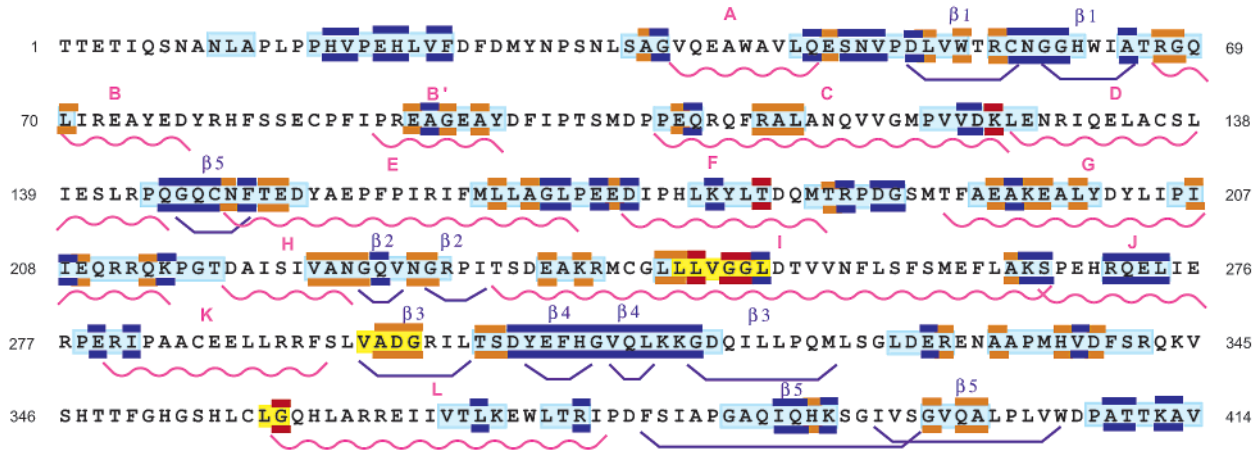

FIGURE 3: Amino acid sequence of CYP101, annotated for secondary structural features, NMR chemical shift assignments, and perturbations due to Pdx addition. Sequence numbers are noted at the beginning and end of each line. Wavy red lines indicate helices, and straight purple lines indicate β-sheets. Secondary structural features are named above the sequence according to the nomenclature of Raag and Poulos (*41*). Residues for which resonance assignments have been made are backgrounded in light blue for Fe(III)S and in yellow if assigned only in CO−Fe(II)S. Dark blue borders indicate resonances that are unperturbed by Pdx addition, those bordered in orange are shifted upon addition of Pdx, and those bordered in red are broadened to invisibility upon the first addition of Pdx.

place in the course of the titration. The cytochrome b_5 solution was originally 3 mM in concentration and was added in two aliquots to 200 μL of a 0.2 mM CO−Fe(II)S NMR sample, resulting in ~5:1 and ~10:1 molar ratios of cyt b_5:CYP101. Experimental conditions were as for the other titrations.

Processing of NMR Experiments. All data was processed using the Bruker XWIN NMR program (version 2.5). XEASY (*24*) was used to assist in the sequential assignments and analysis of the titration data.

Estimation of K_d and Line Shape Analysis for the Pdx^r/CO−Fe(II)S Complex. For five NH resonances that show significant perturbation on the chemical shift time scale and for which resonances are well resolved in all five HSQC spectra, the ^{1}H chemical shifts δ were fitted to the following standard equation using the nonlinear regression analysis package of Mathematica 3.0:

$$\delta = \delta_0 + (\delta_{max} - \delta_0)[K_d + m_0 + p_0 - (K_d + m_0 + p_0)^2 - 4m_0p_0]^{1/2}/2m_0$$

where δ_0 and δ_{max} are the chemical shifts of the free and complexed forms of CYP101, respectively, and m_0 and p_0 are the nominal concentrations of CYP101 and Pdx, respectively. The fits yielded values for δ_{max} and K_d. The reported value of K_d in the text is the average value obtained from the fits, with the error representing the extrema of the values.

Line widths used to estimate state lifetimes were obtained using a Lorentzian deconvolution and line fitting available in XWIN NMR. T_2* for line fitting was estimated from line width measurements and from ratios of relative peak heights after adjustment for concentration changes.

RESULTS

Sequential ^{1}H, ^{15}N, and ^{13}C Backbone Resonance Assignments for Oxidized Camphor-Bound CYP101 [Fe(III)S]. The extent of sequential resonance assignments in CYP101 is shown in relationship to the structure in Figure 3. Sequential assignments of CYP101 were made using a combination of ^{15}N-edited NOESY, HNCA, HN(CO)CA, and HNCACB data. Initially, data for the camphor-bound oxidized (Fe^{3+}) form of the enzyme, Fe(III)S, were obtained. This species is paramagnetic and high spin ($S = {}^5/_2$) and as such cannot be used for sequence-specific assignment of NMR resonances nearer than ~8 Å from the heme iron. Nevertheless, the Fe(III)S form provides a significant advantage for sequential assignments in that sequential NH−NH nuclear Overhauser effects (NOEs) are readily observed in NOESY spectra of uniformly ^{15}N- labeled and perdeuterated Fe(III)S obtained using relatively short (t_m = 150 ms) mixing times. NOESY spectra of similarly isotope-labeled reduced carbon monoxide-bound CYP101 [CO−Fe(II)S] obtained using the same mixing time were less informative, with relatively weak NOE cross-peaks. Longer mixing times gave little improvement of NOESY spectra for CO−Fe(II)S, and spin diffusion was increased. The reason for the difference between the two forms is unclear, although it is possible that the paramagnetism of the metal center provides a sink for magnetization and makes T_1 cross-relaxation (which is responsible for the NOE) more efficient in Fe(III)S relative to T_2 (spin−spin) interactions. At any rate, the combination of through-bond and through-space connectivity provided by the spectra of the Fe(III)S form proved to be invaluable in reducing the ambiguity that arises from a high degree of spectral overlap present in the CYP101 spectrum.

Even with this advantage, the current assignments would have been impossible without the use of extensive selective ^{15}N and ^{13}C labeling. Owing to the difficulty of refolding CYP101, slowly exchanging deuterons in perdeuterated CYP101 samples could not be replaced by protons using denaturation/renaturation. Amide protons are critical for NMR detection of through-bond and through-space connectivities. As such, multiple unpredictable breaks in sequential connectivities were expected. Perdeuterated samples of CYP101 labeled selectively with [^{15}N]glycine, [^{15}N]lysine, [^{15}N]alanine, [^{15}N]leucine, [^{15}N]threonine, [^{15}N]glutamate, [^{15}N]valine, or [^{15}N]tyrosine provided both starting points and confirmatory evidence for sequential ^{1}H and ^{15}N assignments. Although scrambling of ^{15}N labels was observed in some cases, resonance intensity differences and characteristic

$^{13}C_{\beta}$ shifts were usually sufficient to identify such scrambling when it occurred. CYP101 also contains 30 proline residues, which interrupt sequential connectivity by their lack of an NH proton. A perdeuterated sample of CYP101 was prepared, selectively labeled with ^{13}CO-proline and uniformly labeled with ^{15}N. A two-dimensional HNCO experiment performed with this sample provided unambiguous identification of NH resonances that are $i + 1$ relative to prolines.

We believe that the current assignments are the most complete possible using current levels of sample deuteration and magnetic field strengths. All of the data used for these assignments were collected at 14 T (600 MHz ^{1}H) with sample deuteration levels of ~85%. Even with this level of deuteration, $^{13}C\{^1H\}$ dipolar cross-relaxation is efficient enough to degrade multiple-step coherence transfer important for the experiments used for sequential assignments. We are currently preparing samples with more complete deuteration (using perdeuterated ^{13}C sources) which should allow a more complete set of assignments to be obtained.

Resonance Assignments for Reduced Carbon Monoxide- and Camphor-Bound CYP101 [CO−Fe(II)S]. Reduction of CYP101 with sodium dithionite followed by treatment with carbon monoxide (CO) produces the stable diamagnetic reduced CO-bound form of the enzyme, CO−Fe(II)S. The spectral changes resulting from reduction and CO binding to the ^{1}H and ^{15}N spectrum of CYP101 relative to the Fe(III)S form are considerable (Figure 2). Many (even most) of these changes may be due to absence of pseudocontact shifts in the diamagnetic form of the enzyme, although we cannot confirm this as yet. However, the most obvious difference is the appearance of a significant number of new resonances in the ^{1}H,^{15}N HSQC spectrum of CO−Fe(II)S. These resonances correspond to residues in the near vicinity (within 8 Å) of the heme iron of CYP101 and, as such, include most of the active site residues. This contrast provides rapid identification of active site resonances, and we expect that this will become a very general way of examining the active sites of P450 cytochromes using multidimensional NMR methods. We also note that two new resonances appear in the region of the ^{1}H,^{15}N HSQC spectrum of CO−Fe(II)S that corresponds to the $N_{\epsilon}H$ of arginine residues. Only two arginine $N_{\epsilon}H$ protons are within 8 Å of the heme in CYP101. These are the $N_{\epsilon}H$ protons of Arg 112 and of Arg 299. Arg 112 forms a salt bridge with one of the heme carboxylates, while the guanidinium group of Arg 299 forms a tight double hydrogen bond/salt bridge with the other heme carboxylate.

Spectral Changes Observed upon Addition of Pdx to CYP101. The titration of Fe(III)S with Pdx^o does not result in any obvious large changes to the ^{1}H,^{15}N HSQC spectrum of CYP101 [Fe(III)S], as expected, since this nonphysiological complex is relatively weak (*25*, *26*). However, the titration of CO−Fe(II)S with Pdx^r results in considerable spectral perturbation. The response of ^{1}H,^{15}N correlations for CO−Fe(II)S to Pdx^r addition can be divided into three categories. The first category consists of resonances that do not show appreciable chemical shift perturbation ($\Delta\delta_{max} < 10$ Hz) or line width changes upon addition of Pdx^r. The second category consists of resonances that show both chemical shift and line width changes as Pdx^r is added. The perturbations in this category are in fast exchange ($\Delta\delta_{max} < k_{ex}$), although considerable line broadening is observed. The third class includes those resonances that abruptly disappear upon the first addition of Pdx. These represent perturbations that are large enough to fall into the slow-exchange regime ($\Delta\delta_{max} > k_{ex}$). Most of the residues in this class are either in the active site or in close proximity to the heme. The $N_{\epsilon}H$ protons of Arg 112 and Arg 299, residues that form salt bridges with the heme propionates in CYP101, also fall into this category.

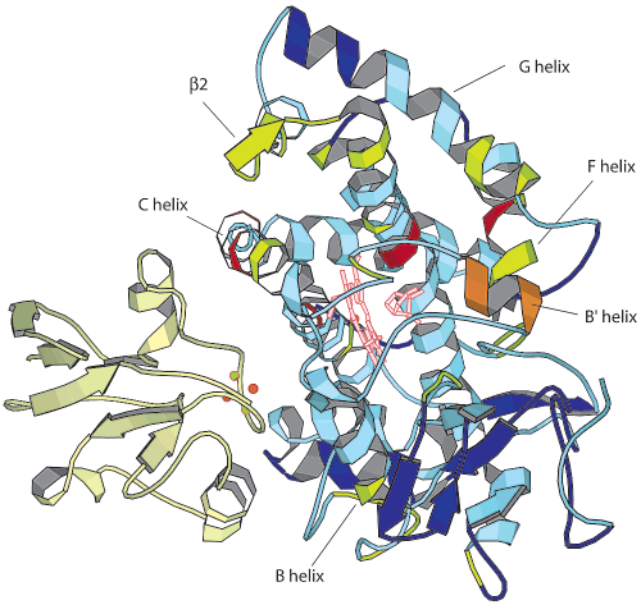

FIGURE 4: Model of the specific complex between Pdx and CYP101 from Pochapsky et al. (*6*). The CYP101 structure is color-coded to show distribution of secondary structural features perturbed by Pdx binding as determined by NMR (see text). Structural features shown in dark blue are not affected by Pdx binding. Those shown in yellow are perturbed ($\Delta\delta_{max} < k_{ex}$), while the resonances of those shown in red disappear abruptly upon addition of Pdx ($\Delta\delta_{max} > k_{ex}$). Note that the $N_{\epsilon}H$ resonances of both Arg residues that interact with the heme carboxylates, Arg 112 and Arg 299, fall into this category (see BMRB database, accession number 5759). The most uniformly perturbed structural feature, the B′ helix (residues 90−96), is shown in orange. Features for which insufficient data are available are shown in light blue. Pdx, in beige on the left, is bound to the proximal face of CYP101. The iron−sulfur cluster is indicated as spheres. Iron atoms in Pdx and CYP101 are shown in orange.

As controls, titrations of CO−Fe(II)S with reduced bovine adrenodoxin and reduced rat cytochrome b_5 were performed. Adrenodoxin, while capable of transferring the first electron to CYP101, is not an effector for CYP101 turnover (*14*). Cytochrome b_5, on the other hand, has effector activity for CYP101, although concentrations required for effector activity are ~20-fold higher than for Pdx (*2*). Perturbations of the CO−Fe(II)S spectrum by Adx^r are within experimental error and do not include any of the marked changes observed upon Pdx^r addition. However, cytochrome b_5 addition perturbs many of the same resonances in CO−Fe(II)S that Pdx^r does, strongly suggesting that the perturbations observed upon Pdx addition are directly related to effector activity. A more complete study of the interactions between CYP101 and cytochrome b_5 is underway.

The structural distribution of Pdx^r-induced perturbations in relation to the proposed complex structure is shown in Figure 4 (*6*). The most perturbed regions of the protein are the N-terminal end of the B helix (residues 66−70), the B′ helix (residues 91−96), the N-terminal end of the C-helix (residues 107−114), both ends of helix E, portions of the F

and G helices, most identified residues in the central I helix, and portions of β-sheets 1, 3, and 5. Relatively unperturbed features include most of the N-terminal residues through residue 35, most C-terminal residues from residue 405 to residue 414, residues in the F/G loop, helices J and K, and β-sheet 4. Secondary structural features not specifically noted here either contain a mix of perturbed and unperturbed residues or do not contain enough assigned residues to determine in which category the feature belongs. In either case, these features are color-coded appropriately in Figure 4.

Nonlinear fits of chemical shift changes for a series of affected resonances as a function of Pdx^r and CO−Fe(II)S concentration give an estimated K_d of 26 ± 12 μM (at 290 K) for complex formation between Pdx^r and CO−Fe(II)S. This agrees well with K_ds calculated from published k_{on} and k_{off} rates for Pdx^r with O_2−Fe(II)S determined by single-turnover kinetics (*27*). Ratios of these rate constants give a K_d ranging from 4 to 30 μM. The lifetimes of the conformational changes enforced by binding of Pdx^r to CO−Fe(II)S can also be estimated from the changes in line width that occur during the course of the titration. If a two-state model (Ef_{on} vs Ef_{off}) is assumed, Lorentzian line fitting for a series of affected resonances yields an estimated bound state lifetime at half-saturation of 3 ms (also at 290 K), which in turn yields an estimate for k_{ex} of ~300 s^{-1}. Fits for residues in various parts of the protein gave approximately the same values for K_ds and state lifetimes, indicating that a two-state model is appropriate for the binding of Pdx^r to CO−Fe(II)S.

Assuming that the Pdx-bound state of CO−Fe(II)S is a good model for the physiological Pdx^r/O_2−Fe(II)S complex, the probability of electron transfer (ET) within the complex must be considerably higher than the observed ET rate (from 0.06 to 0.1 transfers per millisecond) (*27*) in order for ET to take place efficiently during the lifetime of the bound form (~3 ms). However, if the complex geometry in the proposed model is correct, with an intermetal distance of 12 Å (*6*), one might expect a much higher intrinsic electron transfer rate constant. Biological ETs between centers in nondissociating complexes with similar separations often exhibit rate constants between 10^6 and 10^8 s^{-1} (*28*). An intrinsically large electron transfer rate will be masked if that transfer must take place in a relatively short-lived complex (*29*). This would rationalize the observation that, at higher Pdx concentrations, the second electron transfer step is no longer rate limiting (*27*).

DISCUSSION

Role of the Effector in CYP101 Turnover. The most important observation made in the current work is that perturbations induced by the binding of Pdx to CYP101 are not confined to the proximal face of CYP101 (the proposed binding site for Pdx) (*5*−*8*) but encompass many regions of the CYP101 structure. Furthermore, cytochrome b_5 (a known effector for CYP101 turnover) perturbs many of the same resonances that Pdx does, while adrenodoxin (which is not an effector) does not, strongly suggesting that the perturbations are related to effector activity. The long-range conformational effects of Pdx binding on CYP101 suggest that effector activity need not be the result of localized perturbations to the proximal ligand or active site (although these do occur). Effector activity could be the result of selection for a particular subset of conformations of the CYP101 molecule upon effector binding (Figure 5). This model for effector activity would be consistent with the observation that other molecules that do not cause localized spectral perturbations in CYP101 near the heme are capable of acting as effectors for substrate turnover in CYP101. Such molecules would only need to force the conformational selection, without necessarily causing perturbations to the active site, to effect turnover. The model is also consistent with the observation of product evolution in the absence of effector in crystalline CYP101: It is possible that crystal packing forces exert a restraint similar to that exerted by effectors on conformational selection in CYP101 (*30*).

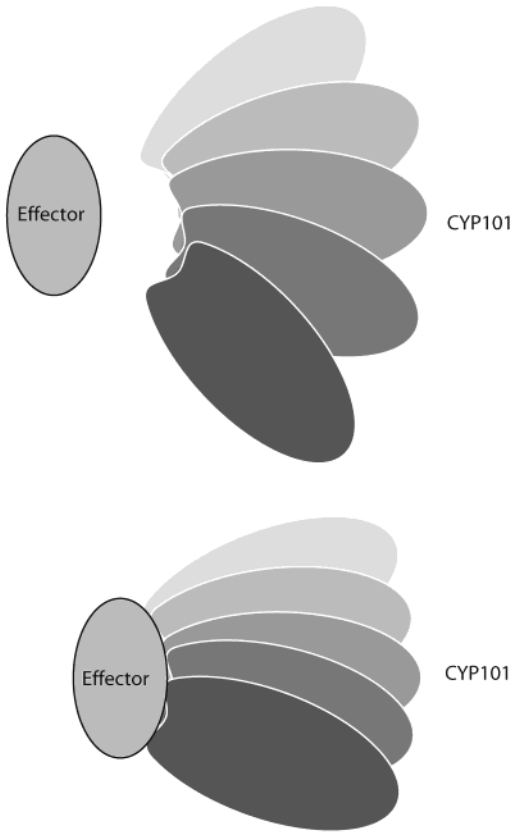

FIGURE 5: Effector binding as a means of enforcing conformational selection. Binding restricts amplitudes of segmental motions, preventing transient opening of substrate/product pathways to the active site.

Ascertaining the role of this conformational selection in allowing turnover is more difficult. However, we note that regions of the protein that have been implicated in substrate access and product egress to and from the active site are perturbed by the binding of Pdx (Figure 4). In particular, the region centered around the B′ helix (residues 90−96) is strongly affected by Pdx binding. This helix and residues in contact with it have been implicated by mutation (*1*), structural analysis (*31*), and dynamics simulations (*32*, *33*) in the control of substrate access into the active site of CYP101. Other evidence suggests that residues in this region are involved in substrate orientation and prevention of uncoupling (*34*, *35*). On the basis of these observations, we propose that the binding of effector restricts the available conformations of CYP101 to those that prevent the loss of substrate and/or intermediate via transiently opened substrate access and egress routes within CYP101. From the observed

patterns of perturbation, it seems likely that the binding of Pdx to the critical residues Arg 109 and Arg 112 causes mechanical displacement of the C helix. This displacement is then transmitted mechanically to the B′ helix either through contacts with the β2 sheet and central I helix or directly through the B/C loop.

The proposed role of the effector in CYP101 turnover (to prevent substrate and/or intermediate loss in the course of the reaction cycle) is consistent with other published results. The regions of CYP101 that are affected by Pdx binding are the same that are found to be perturbed in the crystal structure of CYP101 determined with ruthenium-linker substrates. These substrates force a channel opening between the active site and the surface of CYP101 (*36*). In that work, it was found that the open-channel conformation of CYP101 results in significant displacements of helices G and F, as well as changes in the B′ helix. All three of these secondary structural features are perturbed upon binding of Pdx^r (see Figure 4). Those authors note that, although the F/G loop is displaced in their structures, the conformation of that loop is similar to that of camphor-bound CYP101. This is consistent with our observation of little perturbation in the backbone resonances of the F/G loop.

A mutant of CYP101, D251N, has been described in which the turnover rate is considerably slower than wild type (*37*). The lower activity of D251N CYP101 is ascribed to the inhibition of proton transfer into the active site required for turnover of the enzyme. Nevertheless, binding of Pdx to D251N CYP101 is accompanied by spectral perturbations similar to what is seen in the wild-type complex (*38*). Analysis of oxygen vibrational modes observed in resonance Raman spectra of reduced D251N CYP101/Pdx complexes suggests that the oxygen in the $O_2-Fe(II)S/Pdx^r$ complex is present as $O_2^- - Fe^{3+}$ (superoxide) rather than the two-electron-reduced species $O_2^{2-} - Fe^{3+}$ (peroxide) (*13*). Clearly, electron transfer is also slowed in the D251N complex relative to wild type. The results also indicate that the conformational changes detected upon Pdx binding do not in and of themselves promote electron transfer. Furthermore, heterolysis of the Fe−O bond in the unreduced ($Fe^{3+}-O_2^-$) form would lead to superoxide, the product of $O_2-Fe(II)S$ autoxidation that is observed in the absence of effector (*2*). If effectors act to prevent loss of ligand and/or substrate by preventing the transient opening of access paths to the active site of CYP101, transient dissociation of superoxide from the iron might not automatically result in uncoupling. Instead, the presence of an effector might encourage geminate recombination of transiently dissociated superoxide and eventual turnover.

Another possibility that must be considered is that, if proton and electron transfer are coupled, the effector-enforced conformation might promote efficient proton transfer into the active site. However, we note that neither of the two residues implicated in proton transfer into the active site for which amide resonances have been assigned, Lys 178 and Arg 186 (near the C-terminus of the F helix and within the FG loop, respectively), is perturbed by Pdx binding, despite the fact that some of their near neighbors are perturbed. It is possible that, as our methods report primarily on the effects detected by backbone amides, the side chains of these residues may be affected without perturbing the backbone. Still, while the current data do not rule out a role for effector-induced conformational changes aiding proton transfer, neither do they support it.

Finally, it must be considered that the primary binding mode of Pdx (at the proximal face, as shown in Figure 4) is not the same one that results in effector activity. Multiple binding modes have been suggested for other soluble redox complexes (*39*). The primary arguments against this are the apparently simple two-state nature of the binding that we observe and the lack of effect of surface mutations in CYP101 remote from the proximal site upon activity (*5*, *40*). Still, it is likely that more mutational and spectroscopic work will be required to rule out the possibility of multiple functional binding geometries.

The model for effector activity in the Pdx/CYP101 couple proposed here is appealing in that it complements our dynamic model for modulation of Pdx binding to CYP101 as a function of the Pdx oxidation state. Reduction of Pdx causes a decrease in the conformational freedom of the ferredoxin and increases the binding affinity for Fe(III)S, presumably by decreasing the conformational entropy of Pdx in a manner consistent with CYP101 binding (*6*). There is also evidence that the state of CYP101 affects the binding of Pdx. In the absence of substrate, no change is observed in the EPR spectrum of oxidized CYP101 [Fe(III)] upon addition of Pdx (*10*) nor is there any effect of Pdx upon autoxidation rates of $O_2-Fe(II)S$ unless a substrate analogue is present (*14*). Together, these observations suggest that the specific binding between Pdx and CYP101 is not a passive event for either protein, but a delicate balance of structural and dynamic factors that modulate molecular recognition in this system.

ACKNOWLEDGMENT

The authors thank Huiling Gong for preparing some of the samples used in this work, Prof. Luet-Lok Wong and Dr. Darren Nickerson for the plasmid used for expression of C334A CYP101, Prof. Rita Bernhardt for the plasmid used to express bovine adrenodoxin, and Prof. J. T. J. LeComte for a sample of rat cytochrome b_5.

REFERENCES

1. Mueller, E. J., Loida, P. J., and Sligar, S. G. (1995) in *Cytochrome P450: Structure, Function and Biochemistry* (Ortiz de Montellano, P., Ed.) pp 83−124, Plenum Press, New York.
2. Lipscomb, J. D., Sligar, S. G., Namtvedt, M. J., and Gunsalus, I. C. (1976) *J. Biol. Chem. 251*, 1116−1124.
3. Sligar, S., and Debrunner, P. (1974) *Fed. Proc. 33*, 1256.
4. Pochapsky, T. C., Kostic, M., Jain, N., and Pejchal, R. (2001) *Biochemistry 40*, 5602−5614.
5. Stayton, P. S., and Sligar, S. G. (1990) *Biochemistry 29*, 7381−7386.
6. Pochapsky, T. C., Lyons, T. A., Kazanis, S., Arakaki, T., and Ratnaswamy, G. (1996) *Biochimie* (*Paris*) *78*, 723−733.
7. Roitberg, A. E., Holden, M. J., Mayhew, M. P., Kurnikov, I. V., Beratan, D. N., and Vilker, V. L. (1998) *J. Am. Chem. Soc. 120*, 8927−8932.
8. Unno, M., Shimada, H., Toba, Y., Makino, R., and Ishimura, Y. (1996) *J. Biol. Chem. 271*, 17869−17874.
9. Unno, M., Christian, J. F., Benson, D. E., Gerber, N. C., Sligar, S. G., and Champion, P. M. (1997) *J. Am. Chem. Soc. 119*, 6614−6620.
10. Lipscomb, J. D. (1980) *Biochemistry 19*, 3590−3599.
11. Shiro, Y., Iizuka, T., Makino, R., Ishimura, Y., and Morishima, I. (1989) *J. Am. Chem. Soc. 111*, 7707−7711.

12. Unno, M., Christian, J. F., Sjodin, T., Benson, D. E., Macdonald, I. D. G., Sligar, S. G., and Champion, P. M. (2002) *J. Biol. Chem. 277*, 2547−2553.
13. Sjodin, T., Christian, J. F., Macdonald, I. D. G., Davydov, R., Unno, M., Sligar, S. C., Hoffman, B. M., and Champion, P. M. (2001) *Biochemistry 40*, 6852−6859.
14. Lipscomb, J. D., Sligar, S. G., Namtvedt, M. J., and Gunsalus, I. C. (1976) *J. Biol. Chem. 251*, 1116−1124.
15. Aoki, M., Ishimori, K., and Morishima, I. (1998) *Biochim. Biophys. Acta 1386*, 168−178.
16. Mouro, C., Bondon, A., Jung, C., De Certaines, J. D., and Simonneaux, G. (2000) *Eur. J. Biochem. 267*, 216−221.
17. Mouro, C., Bondon, A., Jung, C., Hoa, G. H. B., De Certaines, J. D., Spencer, R. G. S., and Simonneaux, G. (1999) *FEBS Lett. 455*, 302−306.
18. Banci, L., Bertini, I., Marconi, S., Pierattelli, R., and Sligar, S. G. (1994) *J. Am. Chem. Soc. 116*, 4866−4873.
19. Pervushin, K. V., Wider, G., and Wuthrich, K. (1998) *J. Biomol. NMR 12*, 345−348.
20. Nickerson, D. P., and Wong, L. L. (1997) *Protein Eng. 10*, 1357−1361.
21. Ye, X. M., Pochapsky, T. C., and Pochapsky, S. S. (1992) *Biochemistry 31*, 1961−1968.
22. Uhlmann, H., Beckert, V., Schwarz, D., and Bernhardt, R. (1992) *Biochem. Biophys. Res. Commun. 188*, 1131−1138.
23. Muhandiram, D. R., and Kay, L. E. (1994) *J. Magn. Reson., Ser. B 103*, 203−216.
24. Bartels, C., Xia, T. H., Billeter, M., Guntert, P., and Wuthrich, K. (1995) *J. Biomol. NMR 6*, 1−10.
25. Sligar, S. G., and Gunsalus, I. C. (1976) *Proc. Natl. Acad. Sci. U.S.A. 73*, 1078−1082.
26. Hintz, M. J., Mock, D. M., Peterson, L. L., Tuttle, K., and Peterson, J. A. (1982) *J. Biol. Chem. 257*, 4324−4332.
27. Brewer, C. B., and Peterson, J. A. (1988) *J. Biol. Chem. 263*, 791−798.
28. Moser, C. C., Keske, J. M., Warncke, K., Farid, R. S., and Dutton, P. L. (1992) *Nature 355*, 796−802.
29. Liang, Z. X., Nocek, J. M., Huang, K., Hayes, R. T., Kurnikov, I. V., Beratan, D. N., and Hoffman, B. M. (2002) *J. Am. Chem. Soc. 124*, 6849−6859.
30. Schlichting, I., Berendzen, J., Chu, K., Stock, A. M., Maves, S. A., Benson, D. E., Sweet, B. M., Ringe, D., Petsko, G. A., and Sligar, S. G. (2000) *Science 287*, 1615−1622.
31. Raag, R., Li, H. Y., Jones, B. C., and Poulos, T. L. (1993) *Biochemistry 32*, 4571−4578.
32. Ludemann, S. K., Carugo, O., and Wade, R. C. (1997) *J. Mol. Model. 3*, 369−374.
33. Ludemann, S. K., Lounnas, V., and Wade, R. C. (2000) *J. Mol. Biol. 303*, 813−830.
34. Loida, P. J., and Sligar, S. G. (1993) *Protein Eng. 6*, 207−212.
35. Loida, P. J., and Sligar, S. G. (1993) *Biochemistry 32*, 11530−11538.
36. Dunn, A. R., Dmochowski, I. J., Bilwes, A. M., Gray, H. B., and Crane, B. R. (2001) *Proc. Natl. Acad. Sci. U.S.A. 98*, 12420−12425.
37. Gerber, N. C., and Sligar, S. G. (1994) *J. Biol. Chem. 269*, 4260−4266.
38. Sjodin, T., Christian, J. F., Macdonald, I. D. G., Davydov, R., Unno, M., Sligar, S. C., Hoffman, B. M., and Champion, P. M. (2001) *Biochemistry 40*, 6852−6859.
39. Worrall, J. A. R., Liu, Y. J., Crowley, P. B., Nocek, J. M., Hoffman, B. M., and Ubbink, M. (2002) *Biochemistry 41*, 11721−11730.
40. Lo, K. K. W., Wong, L. L., and Hill, A. O. (1999) *FEBS Lett. 451*, 342−346.
41. Raag, R., and Poulos, T. L. (1989) *Biochemistry 28*, 7586−7592.

BI034263S